Solid Freeform Fabrication 2016: Proceedings of the 27th Annual International Solid Freeform Fabrication Symposium – An Additive Manufacturing Conference
Reviewed Paper

Multi-objective Process Optimization of Additive Manufacturing: A Case Study on Geometry Accuracy Optimization

Amir M. Aboutaleb[1], Linkan Bian[1], Nima Shamsaei[2], Scott M. Thompson[2], Prahalad K. Rao[3]
[1]Industrial and Systems Engineering Department, Mississippi State University, MS, 39762, USA [2]Mechanical Engineering Department, Mississippi State University, MS, 39762, USA
[3]Systems Science and Industrial Engineering Department, Binghamton University-SUNY, NY, 13902, USA

Abstract

Despite recent research efforts improving Additive Manufacturing (AM) systems, quality and reliability of AM built products remains as a challenge. There is a critical need to achieve process parameters optimizing multiple mechanical properties or geometry accuracy measures simultaneously. The challenge is that the optimal value of various objectives may not be achieved concurrently. Most of the existing studies aimed to obtain the optimal process parameters for each objective individually, resulting in duplicate experiments and high costs. In this study we investigated multiple geometry accuracy measures of parts fabricated by Fused Filament Fabrication (FFF) system. An integrated framework for systematically designing experiments is proposed to achieve multiple sets of FFF process parameters resulting in optimal geometry integrity. The proposed method is validated using a real world case study. The results show that optimal properties are achieved in a more efficient manner compared with existing methods.

Key Words

Additive Manufacturing, Multi-objective Optimization, Fused Filament Fabrication, Geometry Accuracy Optimization, Design of Experiments

Introduction

Additive Manufacturing (AM), as a general term, refers to a range of production technologies which fabricates 3D objects from a CAD model directly in a layer upon layer manner [1]. In comparison with traditional subtractive production methods, AM ought to be considered as a manufacturing revolution by virtue of its novel advantages such as allowing for fabricating very complex-shaped and customized parts and handling functionally-graded materials [2, 3]. By emerging Laser-Based Additive Manufacturing (LBAM), now this technology is able to fabricate metal parts, namely stainless steel [4-6], Ti-6-Al-4V[7-9] and nickel-based alloys[10]. In fact, this almost new capacity of AM is a threshold for that to be more applicable for fabricating functional parts in a wide range of high-tech industries such as biomedical, automotive, aerospace and bio-medicine. Despite of all the mentioned advantages, quality and repeatability is still a major barrier for this technology to be applied in a broader scale and applications [11]. In LBAM many controllable process parameters are reported influential on the adhesive powder deposition procedure and the consequential solidification heat transfer during the fabrication process. Accordingly, final part's quality—microstructure and mechanical properties—are strongly dependent upon such process parameters[12]. For instance, laser power, layer thickness, and hatch space between adjacent paths of the laser within the same layer are reported as the most affective controllable process parameters for Selective Laser Melting (SLM) process [13].

Depending on the desired application, fabricated part should possess specific qualities and mechanical properties (or geometric characteristics) such as acceptable level of density, yield strength, ductility, stiffness, elongation to failure, etc. For instance, in biomedical applications, titanium and its alloys such as Ti-6Al-4V are used since they fulfill the major requirements of this application namely low stiffness, high specific strength,

good corrosion and fatigue resistance [14]. Also, open-cell structure of new highly porous metals are recognized very advantageous in orthopedic implants due to their low modules of elasticity and high volumetric porosity, i.e. low density [15]. Additionally, titanium's alloys are vastly employed in aerospace industry applications because of their desired weight saving property resulted from high strength-to-weight ratio [16]. In dental prostheses applications, Ti-Ag and Ti-Cu Alloys are used owing to their relatively high strength for fabricating partial dentures, clasps and bridges [17]. In automotive industry, light-weight materials with acceptable and reliable level of density and strength are required, such as composite materials with high strength and high density [18]. In other cases, depending on the assembly requirements, we need to have parts possessing different geometric characteristics which may not be achieved in a single build.

In many cases, the relationship between various mechanical properties (or geometric characteristics) of the fabricated parts are reported arguably conflicting ones. In other words, the optimal values of different mechanical properties may not be achieved using the same experimental setup. Moreover, due to the high cooling rates of LBAM, the process/design parameters resulting in fabricated parts with high values for one mechanical property (e.g., ductility) may decrease result in low values for other properties (e.g., yield strength). Take Selective Laser Melting, a popular additive manufacturing system for fabricating high quality parts for low to medium quantity, for example. High cooling rate of SLM can cause some problems for ductility of the final part for any metallic powder [9]. In fact, this aspect would be more highlighted when we take the cooling rate's effect on multiple mechanical properties into account. More specifically, to the best of the authors' knowledge, although the high cooling rate during most LBAM processes results in high yield strength, it causes lower ductility or elongation to failure. Considering such existing conflicts among various mechanical properties, it is extremely challenging to identify the optimal process/design parameters that can be used to fabricate parts with acceptable level of various mechanical properties simultaneously. Hence, LBAM process optimization in respect to various mechanical properties should defined as a multi-objective process optimization.

Multi-objective optimization methods could be grouped in two main categories—scalarization or aggregation methods and evolutionary algorithms [19]. Scalarization methods, which represent a classic approach, try to combine all the objective functions with the purpose of converting the multi-objective optimization problem to a single objective one and solve them by routine single-objective optimization problem solvers [20]. This group of methods are not applicable to LBAM multi-objective optimization in that functional form representing the relationship between process parameters and mechanical properties are unknown. On the other hand, evolutionary algorithms iteratively generate a group of potential solutions that represent an acceptable compromises between objective functions [21]. These techniques cannot be applied to LBAM multi-objective problems as well because (i) explicit functional form of objective functions are unknown; and (ii) they need numerous evaluation of candidate solutions which means a huge number of expensive experimental runs in LBAM.

To tackle the aforementioned technical challenges, we propose a novel methodology to optimize LBAM process considering two conflicting objective functions when the objective functions are unknown. In fact, the ultimate goal is to provide the operator or designer with a set of optimum alternatives to select from. Despite the recent advances in AM technologies, it remains an open research area to develop a systematic approach to optimize the AM process of interest for a given material considering multiple mechanical properties required for potential applications.

Problem Definition

The goal of the present research is to optimize an AM process for a given material in respect to two potentially conflicting mechanical properties (or geometric characteristics). For convenience, the objective functions under the study are expressed in the form of maximization as follows:

$$\text{Max}\, \boldsymbol{Y} = \left(Y_1(\boldsymbol{s}), Y_2(\boldsymbol{s})\right)'$$
$$s.t. \quad \boldsymbol{s} \in \boldsymbol{S}$$

$\boldsymbol{Y}$ denotes the vector of objective functions, $\boldsymbol{s}$ is the vector of decision variables (i.e. process parameters); and $\boldsymbol{S}$ denotes the design space. The set of all possible response vectors $\boldsymbol{Y}$ corresponding to the design space is defined as objective space and denoted by $\boldsymbol{C} = \left\{\left(Y_1(\boldsymbol{s}), Y_2(\boldsymbol{s})\right)' \in R^2 : \boldsymbol{s} \in \boldsymbol{S}\right\}$. Note that the optimal process parameters for different objective functions may be completely distinct. In other words, the optimized process parameters for Y_1 may not necessarily result in optimum Y_2 due to the aforementioned potential conflicts among mechanical properties in AM fabricated parts. Improving the response value of one objective function may result in worsening that in another objective function. In fact, all objective functions may not be optimized simultaneously.

Considering different requirements for mechanical properties in different applications, we can define couple of weighting coefficients for objective functions representing the associated relative importance. In that way, the bi-objective optimization problem can be presented as a single-objective problem. For instance, in application *A* we consider 70% and 30% relative importance for mechanical properties Y_1 and Y_2 respectively. In this case the single-objective optimization problem would be expressed in the form of $Max\left(0.7 \times Y_1(\boldsymbol{s}) + 0.3 \times Y_2(\boldsymbol{s})\right)$. However, in many applications the relative importance of mechanical properties are not clearly quantified. In other words, the definition of such weighting coefficients could be subjective in real-world. In addition, considering another application and changing the corresponding relative importance for the mechanical properties, the optimum design parameters will change accordingly in that we have a completely different single-objective function. For example, considering application *B* with 60% and 40% relative importance for mechanical properties Y_1 and Y_2, the optimum solution for problem $Max\left(0.6 \times Y_1(\boldsymbol{s}) + 0.4 \times Y_2(\boldsymbol{s})\right)$ may not be as same as that in the application *A*. More accurately, in many real-world cases simultaneously achieving the optimum solutions for two potentially conflicting mechanical properties may be impossible. Hence, there is no a single optimum solution in these cases. In fact, optimum solution could be a subset of objective space $\boldsymbol{C}$ which can recognize and identify the best trade-off among the conflicting mechanical properties of interest in different applications.

In multi-objective optimization scope a quite different concept of optimality is defined called Pareto optimality. As a matter of fact, Pareto optimal solution is a set of optimum solutions representing the best compromises between various objective functions. Given our bi-objective optimization problem, let define each member of Pareto optimum as a design point $\boldsymbol{s}^* \in \boldsymbol{S}$ if and only if there is no other $\boldsymbol{s} \in \boldsymbol{S}$ such that $Y_k(\boldsymbol{s}) \geq Y_k(\boldsymbol{s}^*)$ for $k = 1, 2$. Here, $\boldsymbol{s}^*$ is called a non-dominated design point and its corresponding response vector as Pareto point $Y_k(\boldsymbol{s}^*)$. We show the Pareto optimum set by $\boldsymbol{E}$. In our bi-objective optimization problem, the Pareto front which is corresponding to response vectors of Pareto set in the objective space $\boldsymbol{C}$ is defined by $\boldsymbol{H}$, that is $\boldsymbol{H} = \left\{\left(Y_1(\boldsymbol{s}), Y_2(\boldsymbol{s})\right)' \in R^2 : \boldsymbol{s} \in \boldsymbol{E}\right\}$. Given two controllable process parameters, the abovementioned concepts are illustrated by Fig 1.

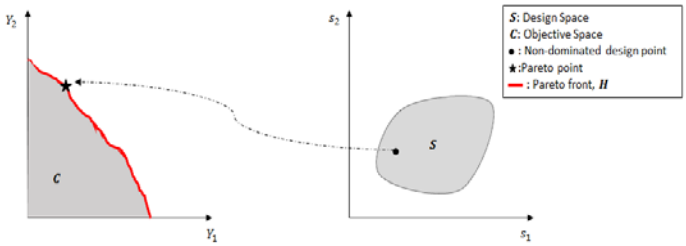

Figure 1. Design Space, Objective Space and Pareto Front

In general, the main goal of solving a bi-objective optimization problem is to attain a reliable approximation of Pareto front by less function evaluation. Optimizing LBAM process for a given material in respect to two potentially conflicting mechanical properties is very challenging for the following reasons:

- The mathematical relation between the mechanical properties of fabricated parts and the process parameters is unknown because of the complexity associated with the underlying thermo-mechanical dynamics of LBAM processes.
- The conflicting mechanical properties may not be optimized simultaneously during the same build.
- The experiments of LBAM are usually very expensive due to high material and machine costs. It may not be economically realistic to conduct a large number of experiments to optimize the process for various applications with different requirements.

In light of the above, there is a great need for developing a novel methodology to achieve the process parameters leading to desired and reliable value of conflicting mechanical properties representing the optimum capacity of given material for LBAM process of interest. In the present research, a novel framework is developed to sequentially design experiments so as to achieve uniformly distributed number of Pareto points on the Pareto front using limited available resources.

Methodology

In this study we develop a novel bi-objective process optimization framework based upon the scalarization concept which tackles the bi-objective optimization problem by systematically solving a sequence of single-objective sub-problems. Master bi-objective problem is divided into various single-objective problems considering different values of weighting coefficients for objective functions. Considering lack of functional form of objective functions and high cost of LBAM experiments, each constructed single-objective sub-problem is optimized by Sequential Minimum Energy Design (SMED) [22]. After optimizing each single-objective optimization problem, updated Pareto points would be identified based on non-domination concept. Then, the appropriate weighting coefficients for the next sub-problem is chosen to lead the next sub-problem optimization in a way that covers largest un-covered part of the Pareto front. Furthermore, after solving each sub-problem, all the resulted experimental results are fed into SMED as prior data to accelerate optimizing of the next sub-problem. This process will continue until the available resource is finished. The proposed method tries to accelerate the bi-objective optimization process by jointly solving the sub-problems in a systematic manner. In fact, the method attempts to map and scale experimental data resulted from previous sub-problems to achieve the optimum for remaining sub-problems with the purpose of efficiently use the limited available resources. The general scheme of the proposed method is illustrated by Fig. 2.

- **Variable Definition**

Denote the experimental data by $(\boldsymbol{s}_i, \boldsymbol{Y}_i)$ for $i = 1, 2, 3, \ldots$ where $\boldsymbol{s}_i$is the ith design point and $\boldsymbol{Y}_i$ is the corresponding response vector, $\boldsymbol{Y}_i = \left(Y_{1_i}, Y_{2_i}\right)'$. Note that upper case letters are used to represent the unknown variables in this paper, while lower case letters are considered for known variables.

- **Sub-problems Construction**

Major bi-objective optimization problem $Max\ \boldsymbol{Y} = \left(Y_1(\boldsymbol{s}), Y_2(\boldsymbol{s})\right)'$ is decomposed into a sequence of single-objective functions, each of which expressed as a convex combination of the objective functions. Each sub-problem could be mathematically expressed as follows:

$$\text{Max } Z^h(\boldsymbol{s}) = \gamma_1^h . Y_1(\boldsymbol{s}) + \gamma_2^h . Y_2(\boldsymbol{s})$$
$$s.t. \quad \boldsymbol{s} \in \boldsymbol{S}$$
$$where \ \gamma_1 + \gamma_2 = 1$$
$$\gamma_k^h \geq 0 \quad for \quad k = 1, 2$$

γ_k denotes weighting coefficient corresponding to the relative importance of the kth objective function within the hth sub-problem. In fact, each sub-problem represents process optimization in respect to a specific application (aerospace, biomedical etc.).

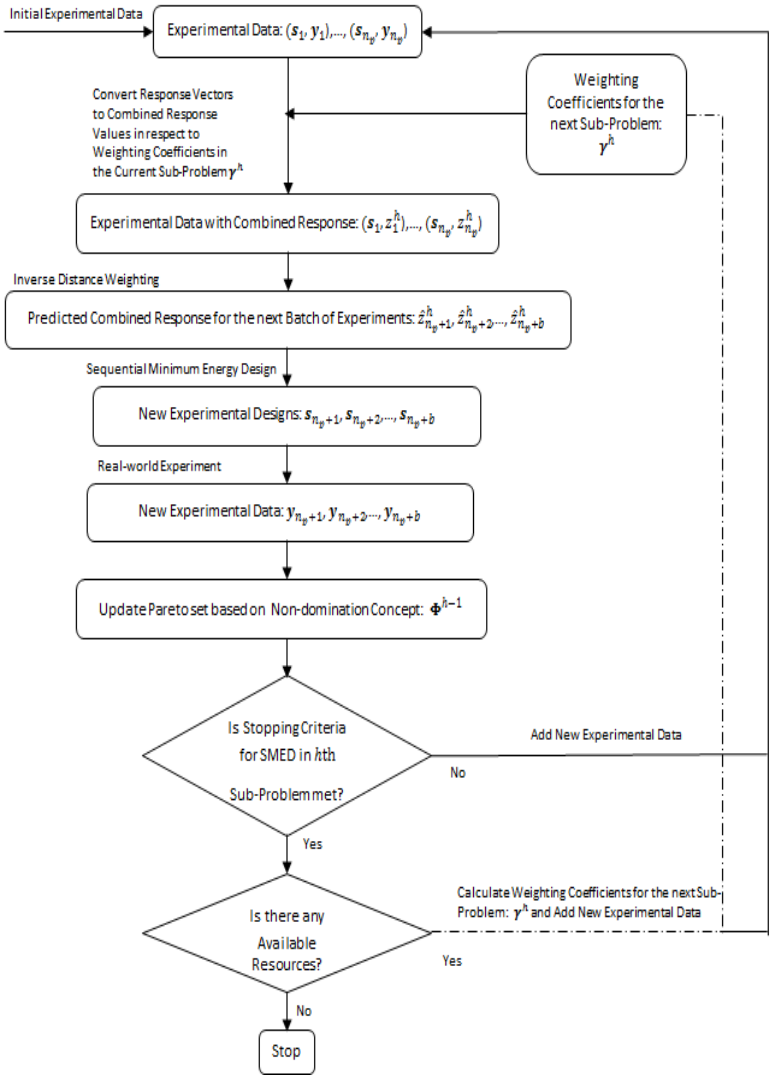

Figure 2. Flowchart of the Methodology

- **Sequential Minimum Energy Design (SMED)**

SMED is applied for optimizing each of the sub-problems. Assuming that weighting coefficients $(\gamma_1^h\ \gamma_2^h)$ are determined, all the design points represented in response vector format, $(\boldsymbol{s}_i, \boldsymbol{Y}_i)$, should be expressed in the form of combined response data as $(\boldsymbol{s}_i, Z_i^h)$ in the framework of SMED. In the rest of the SEMD method detail, the combined response form of the experimental data are applied throughout the algorithm, i.e. $(\boldsymbol{s}_i, Z_i^h)$. Note that all the experimental data attained during the optimization process of prior sub-problems (i.e. sub-problems$1,2,\dots,h-1$) are transformed and fed into the SMED of hth sub-problem as prior data to accelerate optimization process of the current sub-problem by predicting the combined responses in a more accurate manner.

SMED is developed to balance two important properties simultaneously, i.e. optimization and space-filling. For the sake of optimization goal, we should put more design points in the regions of $\boldsymbol{s}$ which more probably can result in maximum value of the response function $Z^h(\boldsymbol{s})$. On the other hand, to avoid being trapped in a local optima, space-filling property should be considered as well. Hence, the range of process parameters with lower chance of optimization ought to be also examined.

In SMED method, a positive electrical charge is assigned to each design point, i.e. $q^h(\boldsymbol{s}_j)$. Selection of the charge function $q^h(\boldsymbol{s})$ relies on the optimization objective. Considering maximization objective in our case, charge function $q^h(\boldsymbol{s})$ should be inversely proportional to the combined response values $z^h(\boldsymbol{s})$. In that way, electrical particles with higher charge would be assigned to design points with lower $z^h(\boldsymbol{s})$ and vice versa. Based on a very fundamental physics law, the charged particles repel each other apart to minimize the total electrical potential energy among them. Hence, design points with lower $z^h(\boldsymbol{s})$, i.e. with higher electrical charge, pushes other design points away more strongly. By contrast, design points with higher $z^h(\boldsymbol{s})$, i.e. with lower electrical charge, allows for more design points to be placed in their neighborhood. The resultant positions of them correspond to the minimum energy designs. In that way, more design points with higher $z^h(\boldsymbol{s})$ values would be selected to sequentially maximize the objective function of interest in the current sub-problem, i.e. $Z^h(\boldsymbol{s})$.

The potential energy between any two design points $\boldsymbol{s}_i$ and $\boldsymbol{s}_j$ is equal to $q(\boldsymbol{s}_i)q(\boldsymbol{s}_j)/d(\boldsymbol{s}_i, \boldsymbol{s}_j)$, where $d(\boldsymbol{s}_i, \boldsymbol{s}_j)$ represents the Euclidean distance between $\boldsymbol{s}_i$ and $\boldsymbol{s}_j$. Hence, total potential energy function within hth sub-problem including ith new design is formulated as follows:

$$E_i^h = \sum_{j=1}^{i-1} \sum_{j'=j+1}^{i} \frac{q^h(\boldsymbol{s}_j) q^h(\boldsymbol{s}_{j'})}{d(\boldsymbol{s}_j, \boldsymbol{s}_{j'})}$$

The new design point can be obtained by solving $\boldsymbol{s}_i = \operatorname{argmin} E_i^h$.

- **Predicting Combined Response at New Design Points**

Due to some real-world applications, we design the experiments in the form of batch to enhance the efficiency of the optimization process in terms of time. Here, the batch size is represented by b which is an integer number. In SMED, Inverse Distance Weighting (IDW) formula is applied for predicting $z^h(\boldsymbol{s})$ values for new design points [22]. Predicted combined responses,$\hat{Z}_i^h$, depend on actual combined response values from previous batch of experiments, i.e. $z_1^h, z_2^h, \dots, z_{\left\lfloor \frac{i-1}{b} \right\rfloor b}^h$. Note that $\left\lfloor \frac{i-1}{b} \right\rfloor b$ is an index showing the number of resulted design points before ith one. Assume that in the current stage of the hth sub-problem a number of prior experimental data are available represented by $(\boldsymbol{s}_i, \boldsymbol{y}_i)$ for $i = 1, 2, 3, \dots, n_p$, where n_p is the number of available data. Clearly, $n_p$is not a fixed number and increases after designing a new batch of experiments by b. By IDW,

predicted combined response of the next batch of experiments are calculated, i.e. $\hat{Z}_i^h$ for $i = n_p + 1, n_p + 2, \dots, n_p + b$. $\hat{Z}_i^h$could be calculated as follows:

$$\hat{Z}_i^h = \frac{\sum_{i'=1}^{\lfloor \frac{i-1}{b} \rfloor b} |\boldsymbol{s}_i - \boldsymbol{s}_{i'}|^{-2} \; z_{i'}^h}{\sum_{i'=1}^{\lfloor \frac{i-1}{b} \rfloor b} |\boldsymbol{s}_i - \boldsymbol{s}_{i'}|^{-2}}$$

where $|\boldsymbol{s}_i - \boldsymbol{s}_{i'}|^{-2}$is a coefficient which determines the effect of $\boldsymbol{s}_{i'}$ and its response value $z_{i'}^h$ on $\hat{Z}_i^h$. Then, predicted combined response for all untested design points are used for calculating the magnitude of the corresponding charged particle and consequently total potential energy E_i^h.

- **Charge Function**

In general, there is not any universal guideline for choosing charge function. However, a positive and decreasing function of the combined response values, $z^h(\boldsymbol{s})$, could be a reasonable choice. Assuming that combined single response values are normalized and fit in the interval [0,1], a possible choice is $q^h(\boldsymbol{s}) = \left(1 - \alpha z^h(\boldsymbol{s})\right)^{\beta}$, where α and β are positive tuning constants with $\alpha \leq [max_{\boldsymbol{s}} z^h(\boldsymbol{s})]^{-1}$[22]. Here we assume that optimum value of each objective is known. This assumption is consistent with our geometric accuracy optimization since there is always an acceptable tolerance in design which ought to be met. Since combined single response values are normalized we can fix $\alpha = max_{\boldsymbol{s}} z^h(\boldsymbol{s}) = 1$.

- **Stopping Criteria**

At one stage of designing experiments within the hth sub-problem the algorithm should automatically shift to the next one by introducing next appropriate vector of weighting coefficients, i.e. ${\boldsymbol{\gamma}_k}^{h+1}$. To do so, contribution of designing experiments within the hth sub-problem should be quantified at first. There are many performance indicators in the multi-objective optimization literature to measure or compare the quality of the resulted Pareto points [23]. In the present methodology, we employ Hyper-Volume (HV) metric as measure of the resulted Pareto points' attainment. By definition, HV is the volume in objective space dominated by resulted Pareto points. In the bi-objective case, HV is the stair-stepped region covered by resulted Pareto points in the objective space. Fig.3. illustrates HV concept in bi-objective case. Light gray area is HV associated with gray Pareto points. ΔHV representing area of dark gray rectangle is contribution of new Pareto point in terms of improvement in HV. Taking the concept of ΔHV into account, the presented algorithm continues designing experiments within the hth sub-problem till we do not see N_{Change} times improvement in ΔHV.

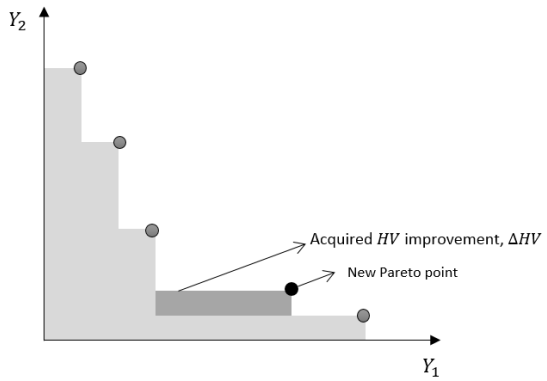

Figure 3. Hyper Volume (HV) and ΔHV

Similarly, proposed algorithm stops continuing introducing further sub-problems and designing more experiments when we do not observe any improvement in ΔHV after designing experiments within N_{Finish} sub-problems. There is no any universal guideline for fixing appropriate N_{Change} and N_{Finish}, hence they should be adjusted depending on the available resources, complexity of the true Pareto front, design space size and the required quality of resulted Pareto points.

- **Weighting Coefficient**

As it has been mentioned before, our final goal is to achieve a uniform coverage of front by solving a sequence of sub-problems. Based on the resulted Pareto points after terminating each sub-problem optimization, weighting coefficients for next sub-problem, $\boldsymbol{\gamma}^h$, is calculated as follows. To initialize the algorithm, weighting coefficients should be predefined for the first two sub-problems as $\boldsymbol{\gamma^1} = (0,1)$, $\boldsymbol{\gamma^2} = (1,0)$**.** By the following procedure, weighting coefficients for the rest of the sub-problems, i.e. $\boldsymbol{\gamma}^h$ for $h = 3,4,5, \ldots$, would be resulted. Assume that after solving $(h-1)$th sub-problem Pareto set $\boldsymbol{\Phi}^{h-1} = \left\{(\boldsymbol{s}^{*^1}, \boldsymbol{y}^{*^1}), (\boldsymbol{s}^{*^2}, \boldsymbol{y}^{*^2}), \ldots, (\boldsymbol{s}^{*^m}, \boldsymbol{y}^{*^m})\right\}$ including m non-dominated design points and corresponding actual response vector is achieved. Then all the existing optimum parameter setups should be sorted in increasing order of $y_1(\boldsymbol{s})$ and relabeled as $\boldsymbol{\Psi}^{h-1} = \{\boldsymbol{s}_1^*, \boldsymbol{s}_2^*, \ldots, \boldsymbol{s}_m^*\}$. At this stage, Euclidian distance between all of the neighboring Pareto points should be calculated as follows:

$$\delta_j = \left|\boldsymbol{y}(\boldsymbol{s}_{j+1}^*) - \boldsymbol{y}(\boldsymbol{s}_j^*)\right| \qquad \text{for} \qquad j = 1, \ldots, (m-1)$$

Then, maximum existing gap on the existing Pareto front is determined by $\Delta = max_{j=1,\ldots,(m-1)}\delta_j$. Two neighboring Pareto points corresponding to Δ are $\boldsymbol{s}_a$ and $\boldsymbol{s}_b$ where $y_1(\boldsymbol{s}_a) < y_1(\boldsymbol{s}_b)$**.** Then, the weighting coefficients for the next sub-problem could be computed as:
$\boldsymbol{\gamma}^h = c^h\left(y_2(\boldsymbol{s}_a) - y_2(\boldsymbol{s}_b)\,,\; y_1(\boldsymbol{s}_b) - y_1(\boldsymbol{s}_a)\right)$, where c^h is a constant leading to $\gamma_1^h + \gamma_2^h = 1$. In that way, algorithm tries to lead forthcoming sub-problems dynamically and intelligently in a path to design more potential experiments in terms of improving resulted Pareto points in an efficient manner.

Numerical Studies

To evaluate and demonstrate effectiveness of the proposed method a series of numerical studies are conducted hereunder. In the simulation study section, the developed methodology is applied to a bi-objective optimization test problem. Furthermore, a real-world case study is done to identify and minimize deviations of major components in geometrical characteristics of Fused Filament Fabrication (FFF) parts. It should be noted that we fixed $\gamma = 3$ in charge function $q(\boldsymbol{s}) = (1 - y(\boldsymbol{s}))^{\gamma}$ for all simulations and case study as the tuned parameter in that it is recommended by [22, 24]. Additionally, stopping criteria parameters are fixed as ($N_{Change} = 10$, $N_{Finish} = 1$) and ($N_{Change} = 2$, $N_{Finish} = 1$) for simulations and case study respectively.

- **Simulation Studies**

To simulate experimental condition, a design space from a common bi-objective optimization test problems is chosen to simulate the real-world AM process. Note that in reality the functional forms of objectives ($Y_1(\boldsymbol{s})$ and $Y_2(\boldsymbol{s})$) are unknown and here we are just presenting them to simulate the real experimentation. We measure the efficiency of the proposed methodology using General Distance (GD) and Proportional HV (PHV) defined as follows:

- *GD (General Distance)* shows that how far the resulted Pareto points are from the true ones. Assuming that at the end of simulation N Pareto points are resulted, GD could be calculated as follows [25]:

$$GD = \frac{\sqrt{\sum_{i=1}^{N} {\varepsilon_i}^2}}{N}$$

Where ε_i represents the minimum Euclidian distance between ith resulted Pareto point and true Pareto points. Hence, $GD = 0$ represents the best situation in which all the resulted Pareto points are exactly true Pareto points.

- *PHV (Proportional Hyper-Volume)* represents proportion of HV associated with all true Pareto points achieved by resulted Pareto points:

$$PHV = \frac{HV(Resulted\ Pareto\ Points)}{HV(True\ Pareto\ Points)}$$

By definition, PHV is a measure within the range of [0, 1] and in the ideal case $PHV = 1$.
The results of the proposed method is benchmarked against an existing and common design-of-experiments method, i.e. Full Factorial Design.
The relationship between process parameters and two objective functions are as follows [26]:

$$\text{Max}\, \boldsymbol{f} = \big(Y_1(\boldsymbol{s}), Y_2(\boldsymbol{s})\big)$$
$$Y_1(\boldsymbol{s}) = 4s_1$$
$$Y_2(\boldsymbol{s}) = g(\boldsymbol{s}) \times \text{h}\big(f_1(\boldsymbol{s}), g(\boldsymbol{s})\big)$$
$$g(\boldsymbol{s}) = 4 - 3\exp\left(-\left\{\frac{s_2 - 0.2}{0.02}\right\}^2\right)$$
$$\text{h}\big(Y_1(\boldsymbol{s}), g(\boldsymbol{s})\big) = \begin{cases} 1 - \left(\dfrac{Y_1(\boldsymbol{s})}{g(\boldsymbol{s})}\right)^4 & if \quad Y_1(\boldsymbol{s}) \le g(\boldsymbol{s}) \\ 0 & Otherwise \end{cases}$$

where $s_1 \in [0, 1]$, $s_2 \in [0, 1]$. A potential design space including 1027 design points is chosen to make a well-spread objective space. Objective space with normalized objective values consists of 25 true Pareto points represented by black dots in Fig. 4. Two black squares represent initial experiments (prior data) in this simulation which are selected randomly. Intentionally initial prior data are chosen from regions very far from Pareto points. The objective space includes convex set of Pareto points with highly dense aggregation of points close to them. Ultimate goal of the simulation study is achieving a set of uniformly spread Pareto points representing the true ones.

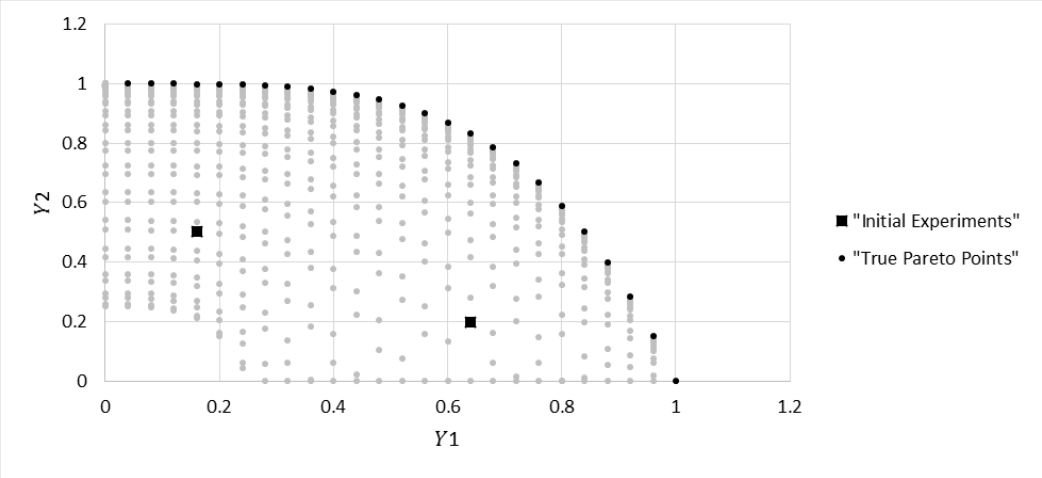

Figure 4. Objective Space, Initial Experiments and True Pareto Points

The conducted sequential experiments by the proposed methodology are illustrated on the objective space by Fig. 5. As it is represented very few of the true Pareto points are not achieved in the test problem.

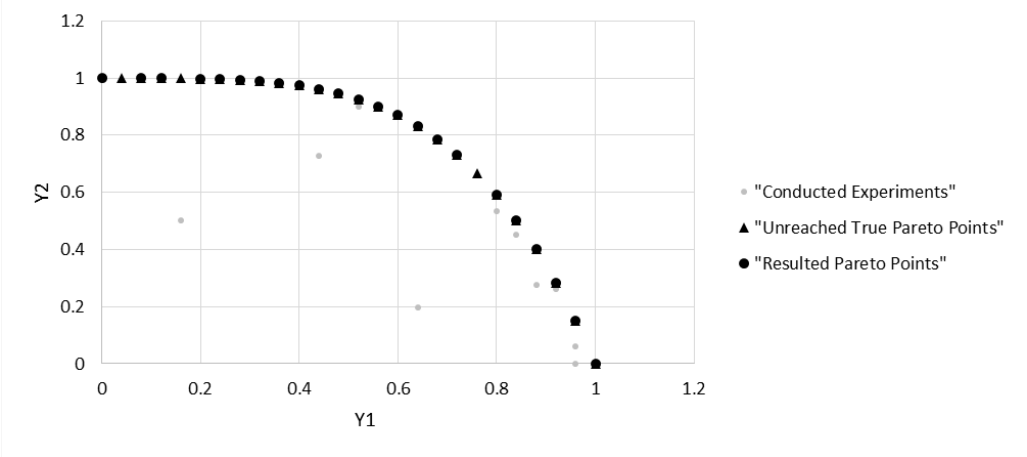

Figure 5. Conducted Simulation Experiments.

We compare our approach with the full factorial design, which is a common technique for optimizing AM processes. Note that experiments of the full factorial design are performed simultaneously, as opposed to our sequential attitude. We vary the number of levels for each of two factors (i.e. s_1 and s_2) to generate a full factorial design resulting in the best possible Pareto points. Note that to fairly compare the performance of the methods we fixed the design space of full factorial designs to the number of experimental runs conducted by the proposed methodology (i.e. 56).

Table 1. Simulation Results

	Number of Conducted Experiments	GD	PHV	PHV Improvement
Proposed Methodology	56	0.001	0.99	7.6 %
Full Factorial Design	56	0.013	0.92	

Based on the results summarized by Table 1, by applying the proposed methodology we achieve GD very close to zero. Furthermore, PHV achieved by the proposed method is very close to one, which is the ideal case. Also, we see significant PHV improvement by applying the proposed methodology compared with full factorial

design. Hence, it could be concluded that the proposed methodology outperforms full factorial design in bi-objective process optimization problems.

Case Study

In this section we apply the proposed method to a real case study which is optimizing deviations in five important geometric features of circle-diamond-square test artifact, Fig.6. The targeted geometric features are as follows: Flatness, Circularity, Cylindricity, Concentricity and Thickness. Two controllable process parameters are considered for design experiments: Infill (%) and Temperature (°C).

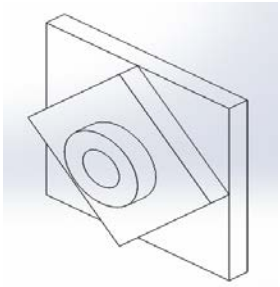

Figure 6. Circle-diamond-square Test Artifact

At the first stage, using experimental data from full factorial design major components within geometrical characteristics of the part is identified by applying Principle Component Analysis (PCA). As the results show, more than 88% variability within the data is captured by the first two principle components (i.e. PC_1 and PC_2). Hence, absolute value of these two PCs are chosen as the objective functions and the ultimate goal is to minimize them.

$$\text{Min } \boldsymbol{PC} = (|PC_1(\boldsymbol{s})|, |PC_2(\boldsymbol{s})|)'$$
$$s.t. \quad \boldsymbol{s} \in \boldsymbol{S}$$

$\boldsymbol{PC}$ denotes the vector of principle components within geometrical characteristics of the part, $\boldsymbol{s}$ is the vector of process parameters; and $\boldsymbol{S}$ denotes the design space.

Table 2. Proportional Variabillity within Principle Components

	$\boldsymbol{PC_1}$	$\boldsymbol{PC_2}$	$\boldsymbol{PC_3}$	$\boldsymbol{PC_4}$	$\boldsymbol{PC_5}$
Standard deviation	1.576	1.3866	0.58981	0.46713	0.16190
Proportion of Variance	0.497	0.3845	0.06958	0.04364	0.00524
Cumulative Proportion	0.497	0.8815	0.95112	0.99476	1

Table 3. PCA Loadings

Rotation	$\boldsymbol{PC_1}$	$\boldsymbol{PC_2}$	$\boldsymbol{PC_3}$	$\boldsymbol{PC_4}$	$\boldsymbol{PC_5}$
Flatness	0.5046	0.2895	-0.7181	-0.3824	0.0481
Circularity	0.5854	-0.1598	0.4859	-0.1831	0.6016
Cylindricity	0.5607	-0.3161	0.1710	0.0901	-0.7404
Concentricity	0.0650	-0.6677	-0.4659	0.5000	0.2877
Thickness	0.2895	0.5895	0.0425	0.7496	0.0687

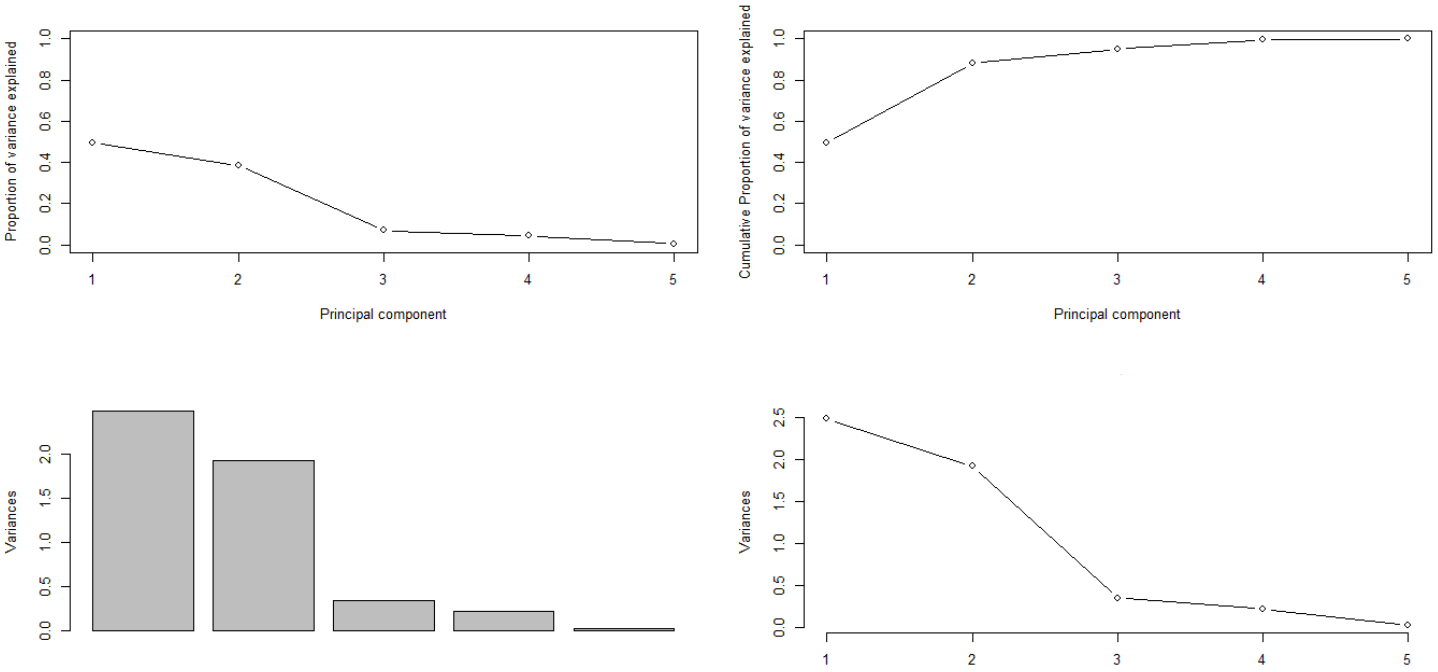

Figure 7. Graphical Demonstration of Proportional Variation within Principle Components

We randomly picked one initial experiment which is very far from the true Pareto points, Fig. 8. By applying the proposed methodology, after conducting 16 experiments in total we achieved three Pareto points. However, to achieve these three Pareto points we need to conduct 20 experiments by applying Full Factorial Design. Hence, 4 experiments are saved compared to Full Factorial Design, i.e. 20% of resources which is a significant improvement. Fig.9 represents the design space including tested and untested experiments by the proposed method compared to Full Factorial Design. Gray design points on the design space represent untested experiments by the proposed methodology.

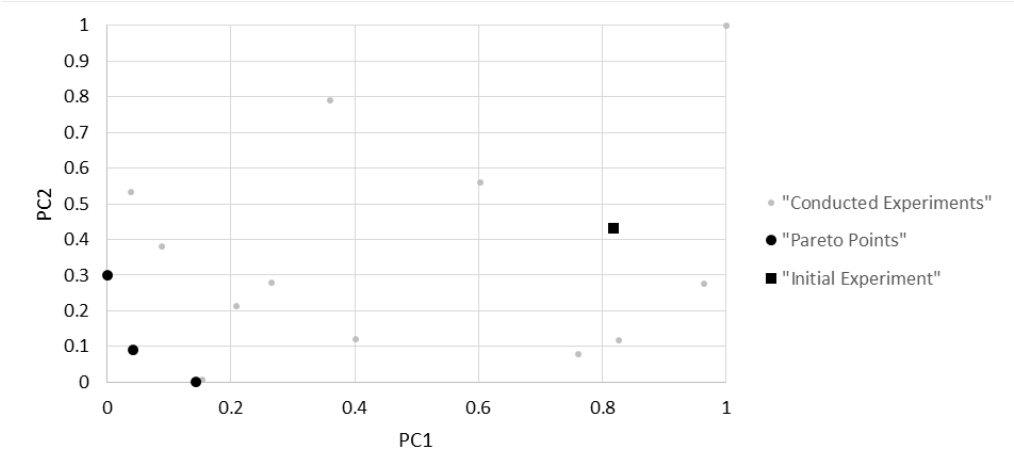

Figure 8. Applying the Proposed Methodology for the Case Study

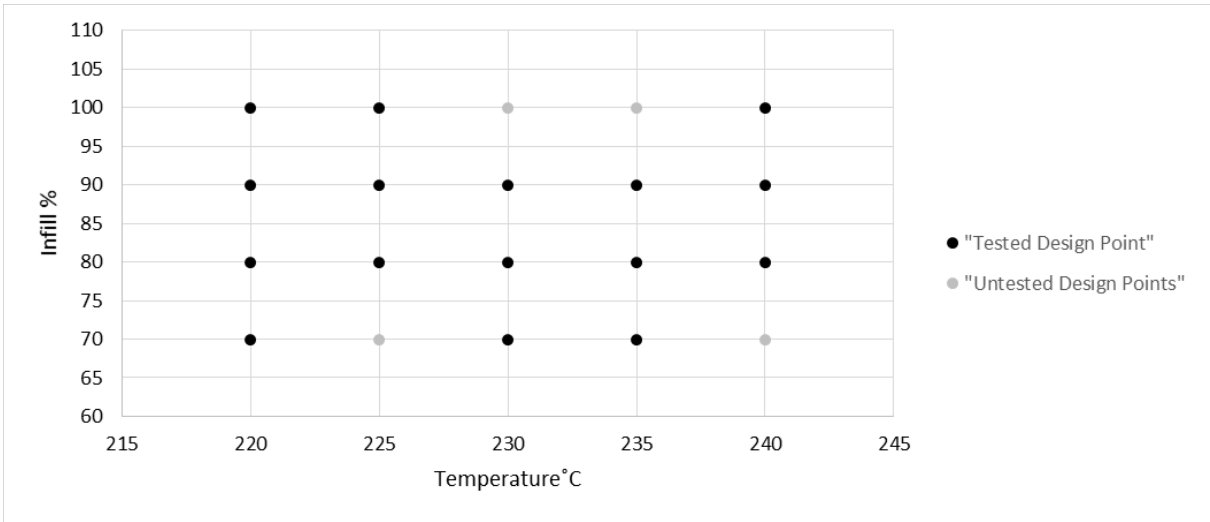

Figure 9. Design Space.

Conclusion

In this paper, a methodology is developed to systematically optimize Additive Manufacturing for multiple objectives (such as different mechanical properties or different geometric characteristics). By jointly solving a sequence of process optimization sub-problems, a set of optimum experimental setups representing the best compromises between mechanical properties (or geometric characteristics) of interest are achieved. Simulation studies and real case study show that our methodology is able to achieve optimum design with significantly less number of experiments compared with Full Factorial Design.

Acknowledgement

This research was sponsored, in part, by grants from the U.S. National Science Foundation (CMMI-1563423).

References

1. L. Bian, S.M.T., N. Shamsaei, *Mechanical Properties and Microstructural Features of Direct Laser-Deposited Ti-6Al-4V.* The Journal of The Minerals, Metals & Materials Society, 2015. **67**(3): p. 629-638.
2. N. Shamsaei, A.Y., L. Bian, S. M. Thompson, *An overview of Direct Laser Deposition for additive manufacturing;Part II: Mechanical behavior, process parameter optimization andcontrol.* Additive Manufacturing. **8**: p. 12-35.
3. S. M. Thompson, L.B., N. Shamsaei, A. Yadollahi, *An overview of Direct Laser Deposition for additive manufacturing; Part I: Transport phenomena, modeling and diagnostics.* Additive Manufacturing, 2015. **8**: p. 36-62.
4. M. Averyanova, P.B., B. Verquin, *Studying the influence of initial powder characteristics on the properties of final parts manufactured by the selective laser melting technology: A detailed study on the influence of the initial properties of various martensitic stainless steel powders on.* Virtual and Physical Prototyping, 2011. **6**(4): p. 215–223.
5. A. B. Spierings, G.L. *Comparison of density of stainless steel 316L parts produced with selective laser melting using different powder grades.* in *Annual International Solid Freeform Fabrication Symposium*. Austin, TX.
6. K. Kempen, E.Y., L. Thijs, J. Kruth, J. Van Humbeeck, *Microstructure and mechanical properties of Selective Laser Melted 18Ni-300 steel.* Physics Procedia, 2011. **12**: p. 255–263.
7. S.J. Li, L.E.M., X.Y. Cheng, Z.B. Zhang, Y.L. Hao, R. Yang, F. Medina, R.B. Wicker, *Compression fatigue behavior of Ti–6Al–4V mesh arrays fabricated by electron beam melting.* Acta Materialia, 2012. **60**: p. 793–802.

8. B. V. Hooreweder, D.M., R. Boonen, J. P. Kruth, P. Sas, *Analysis of Fracture Toughness and Crack Propagation of Ti6Al4V Produced by Selective Laser Melting.* Advanced Engineering Material, 2012. **14**: p. 92-97.
9. S. Leuders, M.T., A. Riemer, T. Niendorf, T. Tröster, H.A. Richard, H.J. Maier, *On the mechanical behaviour of titanium alloy TiAl6V4 manufactured by selective laser melting: Fatigue resistance and crack growth performance.* International Journal of Fatigue, 2013. **48**: p. 300-307.
10. Frazier, W.E., *Metal Additive Manufacturing: A Review.* Journal of Materials Engineering and Performance, 2014. **23**: p. 1917-1928.
11. G. Tapia, A.E., *A Review on Process Monitoring and Control in Metal-Based Additive Manufacturing.* Journal of Manufacturing Science and Engineering, 2014. **136**.
12. L. Bian, S.M.T., N. Shamsaei, *Mechanical Properties and Microstructural Features of Direct Laser-Deposited Ti-6Al-4V.* Journal of Materials, 2015. **67**: p. 629–638.
13. Elsen, M., *Complexity of Selective Laser Melting: a new optimisation approach*. 2007, KATHOLIEKE UNIVERSITEIT LEUVEN.
14. L. E. Murr, S.M.G., F. Median, H. Lopez, E. Martinez, B. I. Machado, D. H. Hernandez, L. Martinez, M. I. Lopez, R. B. Wicker and J. Bracke, *Next-generation biomedical implants using additive manufacturing of complex, cellular and functional mesh arrays.* Philosophical Transactions of the Royal Society, 2010. **368**(1917): p. 1999-2032.
15. F. Matassi, A.B., L. Sirleo, C. Carulli, M. Innocenti, *Porous metal for orthopedics implants.* Clinical Cases in Mineral and Bone Metabolism, 2013. **10**(2): p. 111-115.
16. Boyer, R., *An overview on the use of titanium in the aerospace industry.* Materials Science and Engineering, 1996. **213**(1-2): p. 103-114.
17. M. Takahashi, M.K., Y. Takada, *Mechanical Properties and Microstructures of Dental Cast Ti-Ag and Ti-Cu Alloys.* Dental Material Journal, 2002. **21**(3): p. 270-280.
18. S. C. Tung, M.L.M., *Automotive tribology overview of current advances and challenges for the future.* 2004. **37**(7): p. 517-536.
19. Sh. Deshpande, L.T.W., R. A. Canfield, *Pareto Front Approximation Using A Hybrid Approach.* Procedia Computer Science, 2013. **18**: p. 521-530.
20. Eichfelder, G., *Adaptive Scalarization Methods in Multiobjective Optimization (Vector Optimization)*. 2008: Springer.
21. A. Abraham, L.J., R. Goldberg, *Evolutionary multiobjective optimization: theoretical advances and applications*. 2005: Springer.
22. Dasgupta, T., *Robust Parameter Design for Automatically Controlled Systems and Nanostructure Synthesis*. 2007, Georgia Institute of Technology.
23. E. ZITZLER, L. T., M. LAUMANNS, C. FONSECA, V. DA FONSECA. *Performance assessment of multiobjective optimizers: an analysis and review*. IEEE Transactions on Evolutionary Computation,2003. **7,** 117-132.
24. A. M. ABOUTALEB, L. Bian, A. ELWANY, N. SHAMSAEI. S. M. THOMPSON, G. TAPIA 2016. *Accelerated Process Optimization for Laser-Based Additive Manufacturing by Leveraging Similar Prior Studies*. IIE Transactions. 2016.
25. J. Ryu, S.K., H. Wan, *Pareto Front Approximation with Adaptive Weighted Sum Method in Multi-Objective Simulation Optimization*, in *Winter Simulation Conference*. 2009.
26. C. AUDET, G. S., W. ZGHAL 2008. *Multiobjective optimization through a series of single-objective formulations.* SIAM Journal on Optimization, 2008. **19,** 188-210.